Iranian Journal of Geophysics, 2016, Vol. 9, No. 5, Page 81-92

Rupture characteristics of the 2012 earthquake doublet in Ahar-Varzagan region using the Empirical Green Function method

Hesaneh Mohammadi[1], Mohammadreza Gheitanchi[2*]

[1]*M.Sc. Student of Geophysics, Islamic Azad University, Tehran North Branch, Iran*
[2]*Professor, Earth Physics Department, Institute of Geophysics, University of Tehran, Iran*

(Received: 25 April 2015, accepted: 02 January 2016)

Abstract

On August 11, 2012, within several minutes, two shallow destructive earthquakes with moment magnitudes of 6.5 and 6.4 occurred in Varzagan, Azerbaijan-e-Sharghi Province, in the northwest of Iran. In this study, the Empirical Green Function (EGF) method was used for strong ground motion simulation to estimate the source parameters and rupture characteristics of the earthquakes. To simulate the first earthquake, two aftershocks with magnitudes of 5.6 and 5.2 were used as the EGFs. In the second event, an aftershock with a magnitude of 5 was used as the small event. The size of the main fault caused by the first event was about 18 km in length and 10 km in width. Also, the size of the asperity in the second earthquake was about 16 km in the strike direction and 11 km in the dip direction. The durations of the ruptures in the first and second events were more than 9 and 10s, respectively. The estimated fault plane solution showed strike-slip faulting for the first earthquake and a reverse mechanism with a strike-slip component for the second one. Strike, dip and rake of a causative fault of the first and second earthquakes were determined as 270, 81 and 175 degrees and 230, 57 and 134 degrees, respectively. In addition, the stress drop in the first and second events was calculated to be about 22 and 34 bar, respectively.

Key words: Rupture characteristics, strong ground motion, Ahar-Varzagan earthquake doublet, Empirical Green Function

1 Introduction

On August 11, 2012, within 11 minutes, two shallow destructive earthquakes with moment magnitudes of 6.5 and 6.4 occurred in Varzagan, in Azerbaijan-e-Sharghi province, northwestern Iran. Over the past 40 years, seven earthquakes of magnitudes 6 or greater have occurred within 300 km of the epicentral region.

Global statistics of earthquake pairs reveal strong clustering in space and time, in which the occurrence of one earthquake increases the probability of the second one with a probability decaying with time and distance from the first event (Kagan and Jackson, 1991). There is no clear definition of an earthquake doublet or multiplet. A doublet is usually defined, somewhat arbitrarily, as a pair of events with a magnitude difference of less than 0.2 units, spatial separation less than 100 km, and temporal separation of a few years (Lay and Kanamori, 1980; Astiz and

*Corresponding author: mrghchee@ut.ac.ir

Kanamori, 1984), depending on how large the considered events are. To explore how a doublet may occur, two possible hypotheses are considered. First, the strain could have been released and then accumulated soon or immediately after the first event occurred. The second possibility is that the seismic energy of the second earthquake had been stored within an isolated volume at the vicinity of the first one (Lin et al., 2008).

The earthquake doublet discussed in this paper, had similar magnitudes (less than 0.2), relatively short delays between the two events and occurred within a short distance of each other. The epicenter of the first event was determined as 46.87°E and 38.49°N, the epicenter of the second earthquake was located in 46.73°E and 38.45°N. The second event occurred in the same region, but it was reported that the focal depth of the first earthquake was more than that of the second one. The main shocks were recorded by 66 digital SSA-2 near source strong motion stations. The Peak Ground Acceleration (PGA) of the first and second earthquakes was recorded in Sattarkhan Dam and Varzagan stations, respectively. These events caused structural damage and loss of life. The structures in this region were highly vulnerable to earthquake shaking, though some resistant structures existed. Reportedly, these earthquakes resulted in over 500 fatalities. Also, more than 4000 aftershocks were recorded by the local seismic network, with a maximum magnitude of 5.6.

In this study, the Empirical Green Function method was applied to simulate strong ground motions in order to estimate source parameters such as the seismic moment, corner frequency; duration and rupture characteristics of these earthquakes (Miyake et al., 2000).

2 Data analysis

In this study, near-source data recorded by 66 accelerometers were used to estimate the source parameters. Ground motions recorded at distances within a few fault lengths are called near source data. Near source ground motion records contain better signatures of the spatial and temporal distribution of slip since these are highly influenced by the seismic source effects such as directivity, near source pulse motion and static offsets (Raghu, 2008). Before using accelerograms, data processing is necessary; it includes baseline correction and filtering. Divergence from the base line was resolved by a linear correction. Also, on each component of the accelerogram and for each station, we applied a filter to the raw signal; by a Butterworth filter of the fourth order, the data were band-pass filtered between 0.5 and 25Hz for the first event and between 0.7 and 25Hz for the second event. This filtering helped baseline correction too; the displacement diagram in Varzagan station, before and after processing, is shown in Figure 1.

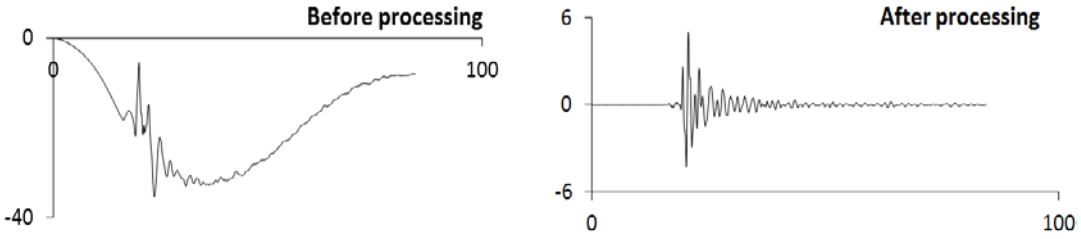

Figure 1. The displacement diagram of the first event in Varzagan station, before and after processing.

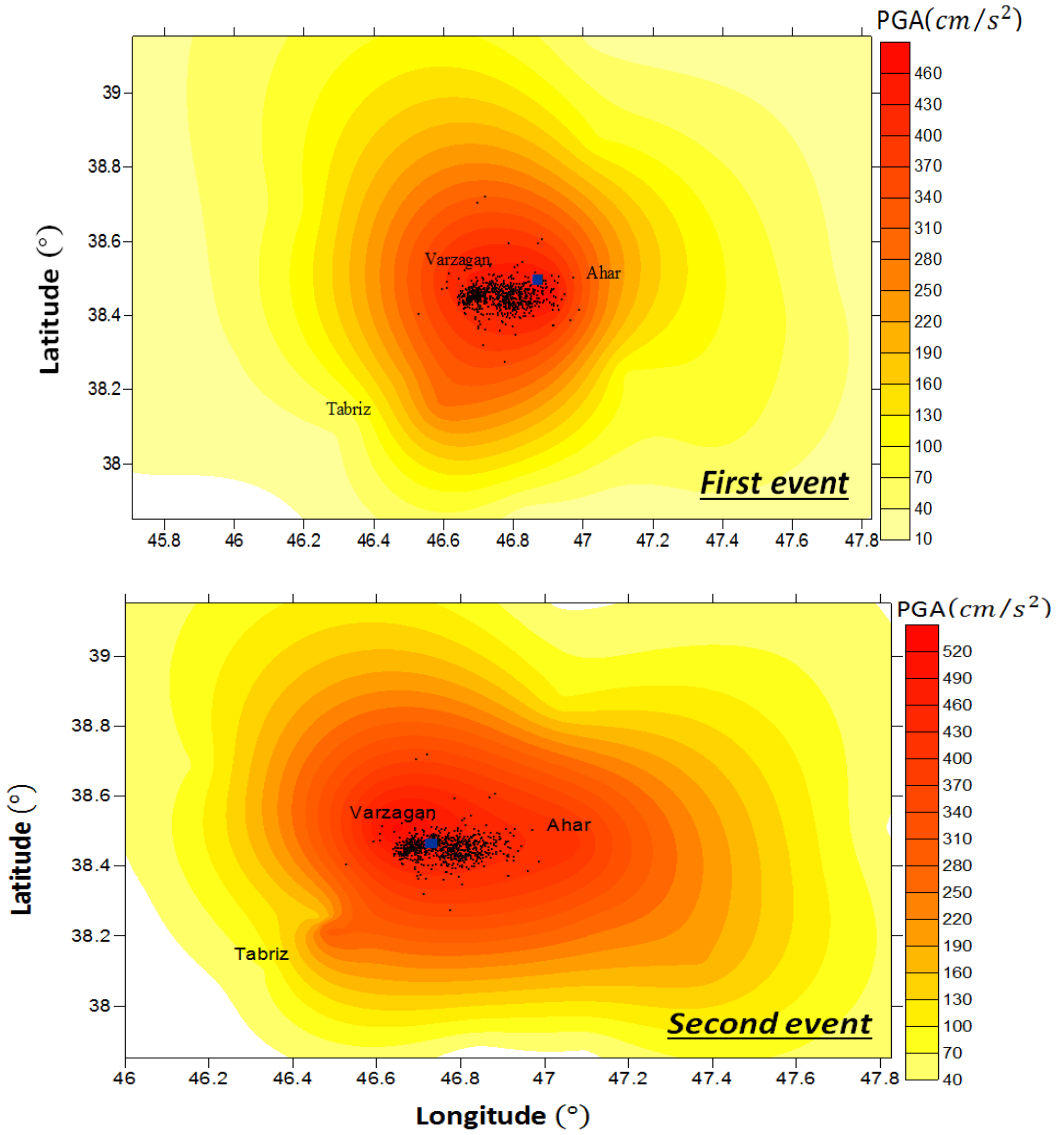

Figure 2. The distribution of aftershocks and spatial distributions of PGA corresponding to the Ahar-Varzagan earthquakes.

Table 1. The parameters estimated from the Fourier spectra.

	Corner frequency (HZ)	**Seismic moment** (N.M)	**Stress drop** (BAR)
First event	0.5	6.705×10^{18}	22
Second event	0.7	3.820×10^{18}	34

Table 2. The parameters of fault planes.

	Fault length in strike direction (km)	**Fault length in dip direction** (km)	**Sub fault length** (km)	**Sub fault width** (km)	**Number of elements in strike direction**	**Number of elements in dip direction**
First event	18	10	2	4	9	**3**
Second event	16	11	2	4	8	**3**

To calculate the stress drop, the corner frequency and seismic moment were determined using Fourier Spectrum on a logarithmic scale (Eshelby, 1957). The parameters estimated from the Fourier spectra are shown in Table 1. Using Peak Ground Accelerations (PGA) recorded by 66 near-field stations, the distribution of PGAs corresponding to the both events was estimated. The spatial distributions of the PGAs corresponding to the Ahar-Varzagan pair of earthquakes and the distribution of about 800 aftershocks are shown in Figure 2. This figure shows that the intensity of the second event was more than that of the first one. Also, the distribution of the aftershocks indicates a rupture from East toward West direction.

3 The empirical Green function method

The Empirical Green Function (EGF) method suggested by Hartzel (1978) is one of the popular and widely used methods of simulating strong ground motions. This method has been widely applied to a large number of earthquakes ranging from moderate $(M_W = 5)$ to very large $(M_W = 8)$ events, using local network data.

During the last twenty years, EGFs have been widely used in earthquake source studies, crustal attenuation studies, strong ground motion prediction, finite rupture modeling, and site-response studies (Mueller, 1985). Theoretically, Green functions are the impulse response of the medium, and EGFs are records used to provide this impulse response (Hutchings and Viegas, 2012). In this technique, an element event is used to simulate the target (main) event. An element (small) event is a foreshock or aftershock of the earthquake (Cheng and Huang, 2011). The EGF method shows that the recordings of small events contain the propagation characteristics, which are necessary for modeling nearby large earthquakes. Therefore, the yielded EGFs are more appropriate than the synthetic seismograms generated by modeling the wave propagation in an inadequately known structure (Courboulex et al., 1996). Using small earthquakes to provide EGF for synthesizing larger earthquakes is quite practical; small earthquakes occur more frequently than the larger ones and the EGF can be readily obtained in a short period before a large earthquake occurs. The focal mechanism of the element event should be similar to that of the target event (Irikura, 1991). The EGF method assumes that the two events have the same hypocenter. Consequently, waves that radiate from the nucleation points of the two events should cross the same medium (Courboulex et al., 1996). To find small events for which this technique can be applied, several criteria were defined. In the search for potential candidates of the earthquake couples, the following criteria were used: The difference in magnitudes must be larger or equal to 1. Both events must be recorded at a minimum of three common stations. The stations must be well distributed in the azimuth around the epicenter. The epicenter of a small event must be located as close as possible to that of the main event. The small events sources are assumed as a point source and they behave like a pulse.

In this study, according to the above criteria, two of the prominently recorded aftershocks with magnitudes of 5.6 and 5.2 were selected as the EGFs for the first earthquake. Also, an aftershock with a magnitude of 5 was used as the small event in the second earthquake. The focal mechanism of the earthquakes and their

aftershocks selected as Green functions are shown in Figure 3.

In this study, the fault rupture dimensions were calculated using the equations estimated by Wells and Coppersmith (1994). The sizes of the main fault and the sub-faults were estimated according to the rupture area of the main event and small event, respectively. In this technique, the main causative plane is divided into sub-faults of equal size. The number of the sub-faults was calculated using the magnitude of the small events. The parameters of fault ruptures generated during these two events are shown in Table 2. Also, the causative fault plane models of the first and second event are shown in Figure 4.

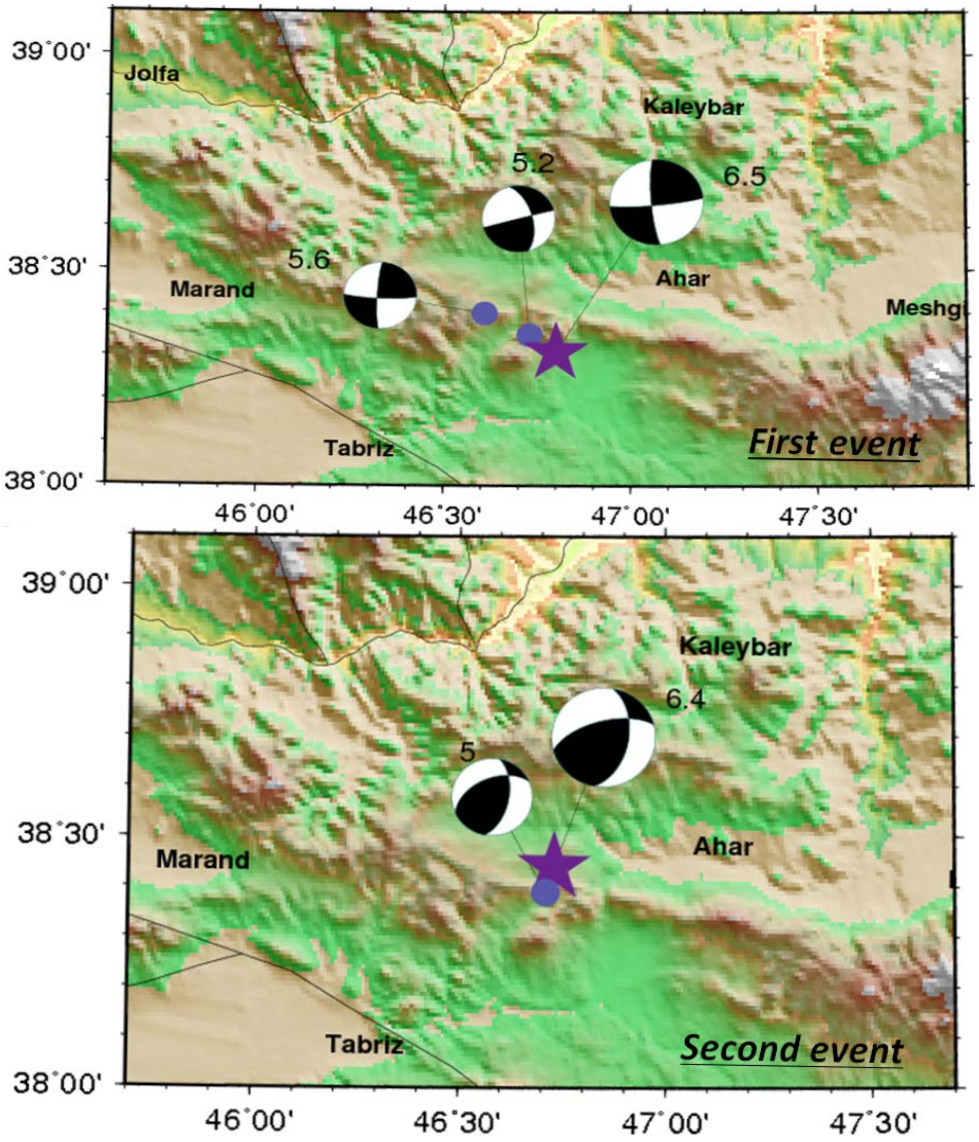

Figure 3. The focal mechanism of the main events and their aftershocks selected as Green functions.

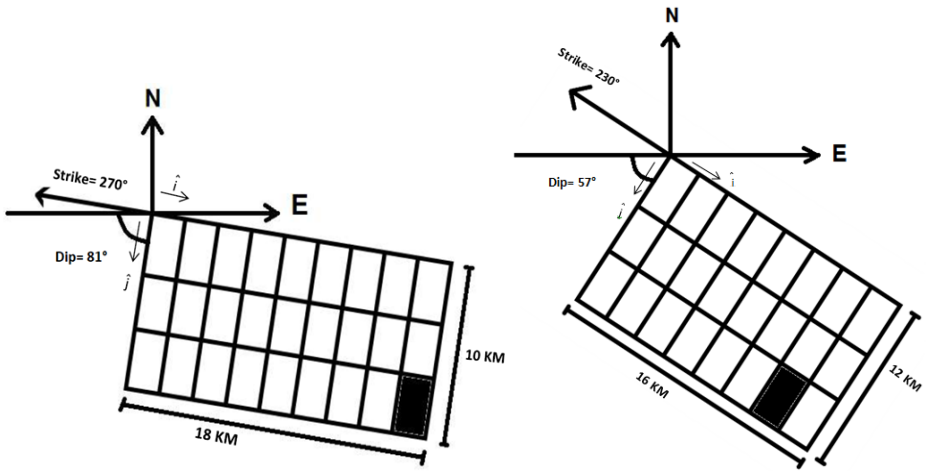

Figure 4. The causative fault plane models of the first earthquake and the second one.

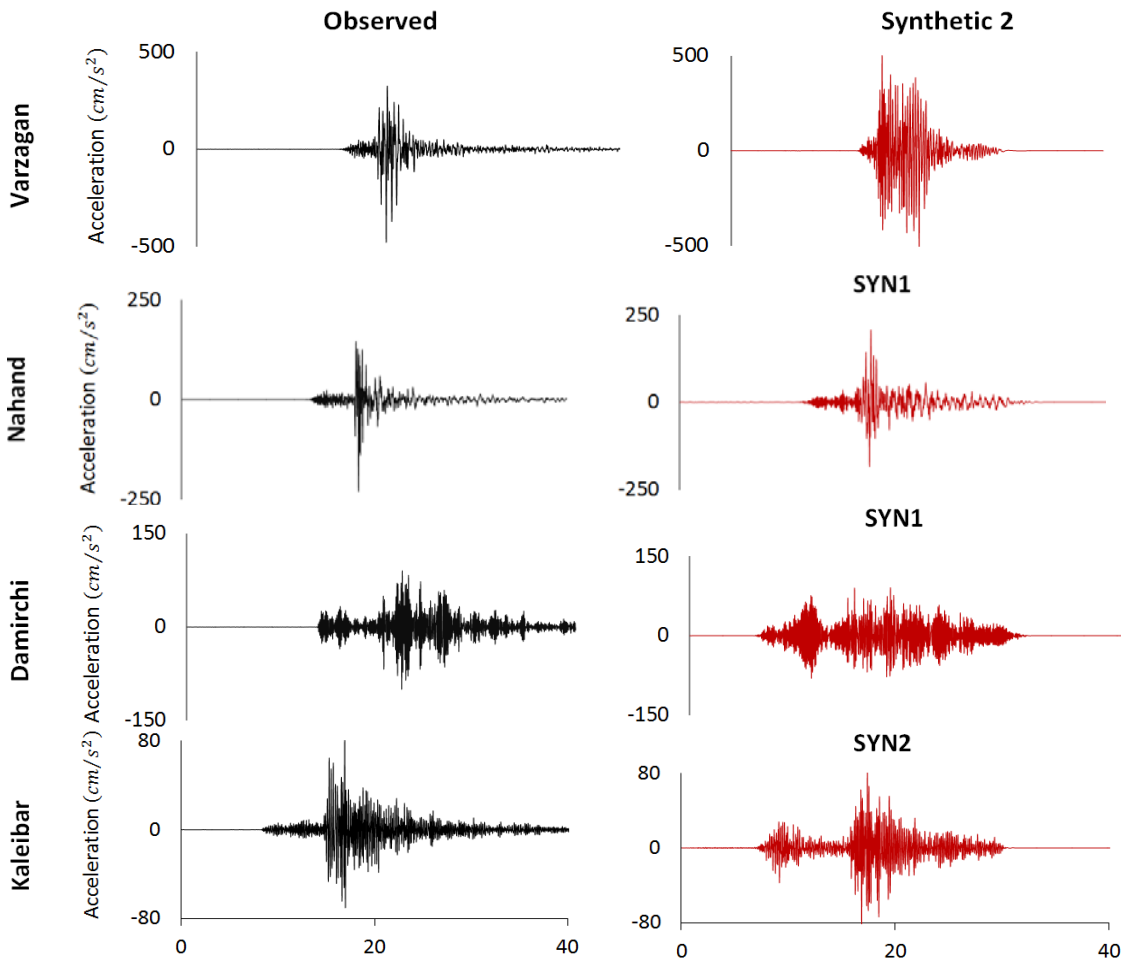

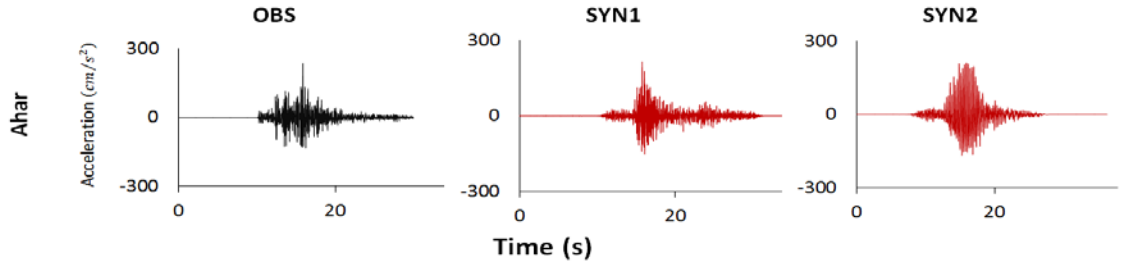

Figure 5. Observed and synthetic acceleration diagrams of the first event in the L component of the near field stations. SYN 1 and SYN 2 are related to the syntheses using aftershocks with magnitude 5.2 and 5.6.

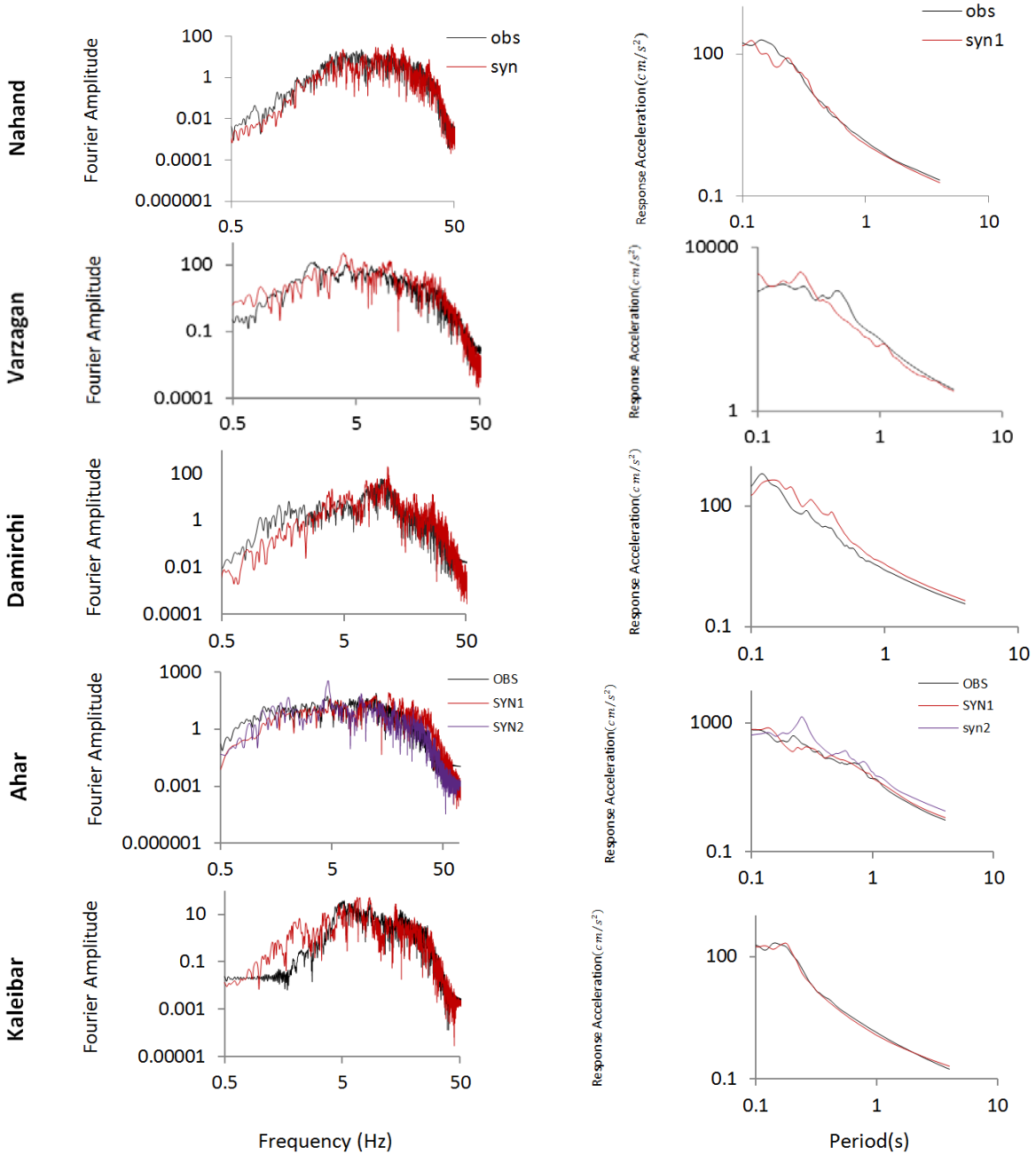

Figure 6. Observed and synthetic Fourier and response spectra of the first event. SYN 1 and SYN 2 are related to the syntheses using aftershocks with magnitude 5.2 and 5.6.

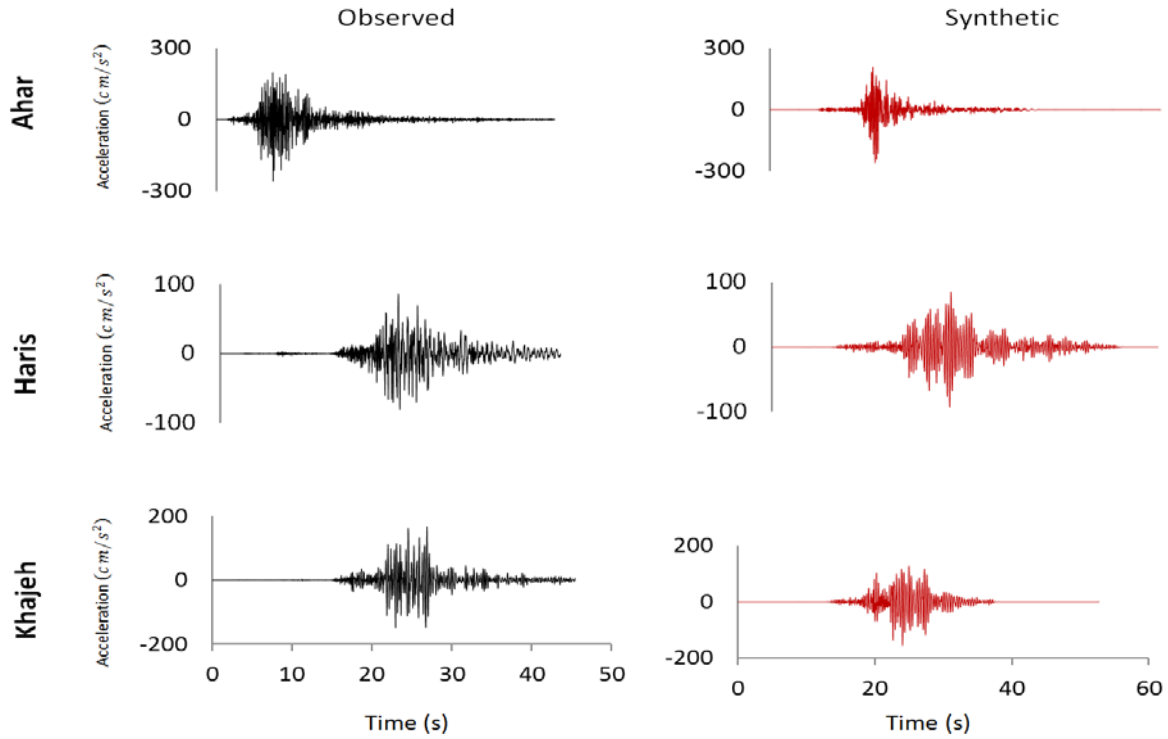

Figure 7. Observed and synthetic acceleration diagrams of the second event (L component).

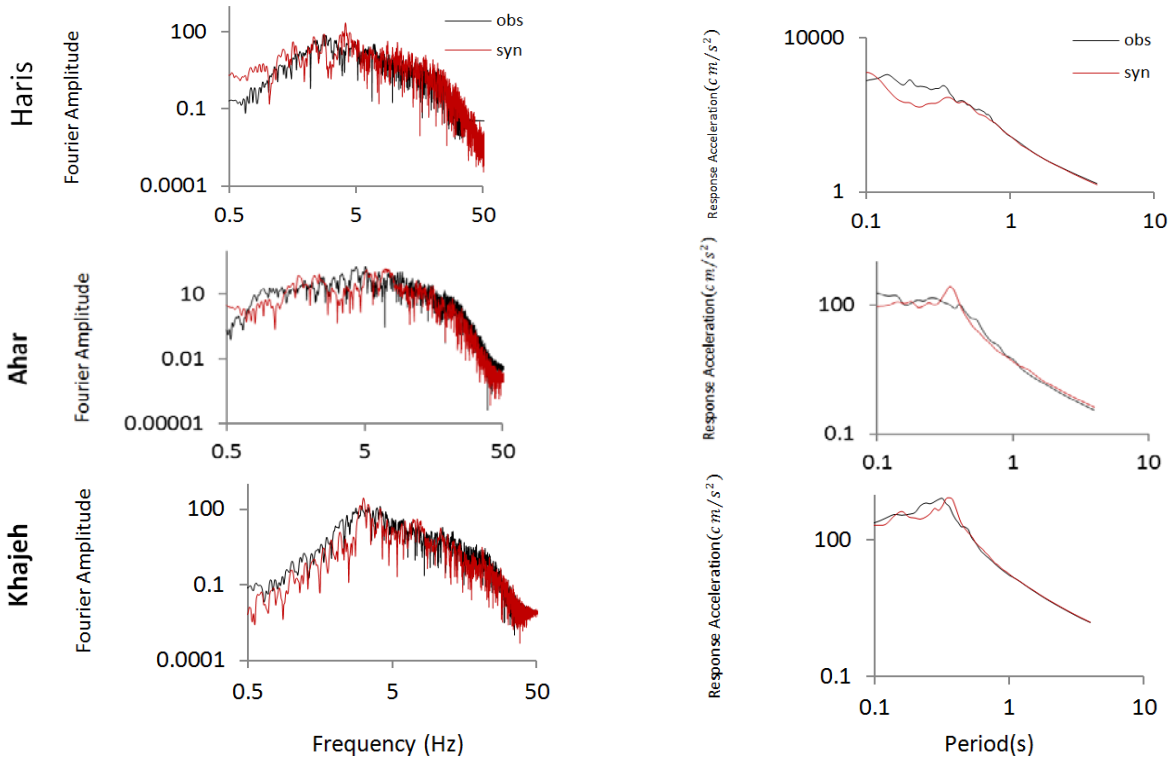

Figure 8. Observed and synthetic Fourier and acceleration response spectra of the second event in the L component of the stations.

Table 3. The peak values of the observed and simulated records of the first earthquake.

station	parameter	Observed			Synthetic 1			Synthetic 2		
		L	T	V	L	T	V	L	T	V
Ahar	PGA(cm/s^2)	210.51	258.19	82.80	212.76	282.08	80.35	210.59	246.81	75.35
	Duration(S)	7	6	13	9	9	12	5	9	13
Damirchi	PGA(cm/s^2)	100.06	84.84	37.55	91.01	92.98	59.05	-	-	-
	Duration(S)	14	16	19	16	16	20	-	-	-
Nahand	PGA(cm/s^2)	229.94	149.01	76.37	207.47	131.72	63	-	-	-
	Duration(S)	6	8	8	8	10	10	-	-	-
Varzagan	PGA(cm/s^2)	479.34	314.87	246.8	-	-	-	528.80	311.84	285.3
	Duration(S)	3	5	5	-	-	-	4	5	5
Kaleibar	PGA(cm/s^2)	80.92	52.20	56.64	-	-	-	84.21	62.19	67.67
	Duration(S)	10	11	12	-	-	-	14	13	12

Table 4. The peak values of the observed and simulated records of the second earthquake.

station	parameter	Observed			Synthetic		
		L	T	V	L	T	V
Ahar	PGA(cm/s^2)	259.80	513.82	123.22	259.40	488.84	138.82
	Duration(S)	8	6	10	3	4	4
Haris	PGA(cm/s^2)	93.15	146.02	51.82	85.81	132.89	55.19
	Duration(S)	13	10	13	13	15	20
Khajeh	PGA(cm/s^2)	166.41	238.26	74.01	155.14	231.48	68.96
	Duration(S)	9	8	13	9	8	12

Using these fault rupture models, a strong ground motion simulation was carried out. The accelerograms of two aftershocks in three components of five stations were used as the input motions to simulate the first main shock records.

Also, the data of the small event in three stations were used to simulate the second earthquake using the summation procedure of the EGF method. The observed and synthetic diagrams of the first event in five ground motion stations and the Fourier and response spectra in logarithmic scale are shown in Figures 5 and 6, respectively. The simulated and observed records in three near source stations of the second main shock, in the time domain, are shown in Figure 7. Also, the Fourier and response spectra of the second earthquake are shown in Figure 8. The peak values of the observed and simulated records of the first and second events are shown in Tables 3 and 4, respectively.

4 Discussion and conclusions

In this study, the EGF method was used; since, the crustal structure is undefined in this area. Furthermore, theoretical methods based on regional 1D crustal models may not accurately identify the complicated propagation effects along the seismic-wave travel path. However, in the EGF method, the waves of small event reaching a given station follow the same ray paths as the main event. Therefore, the EGF methodology provides a superior alternative to the use of other techniques for these earthquakes in this area. The EGF method has been successfully applied in simulating strong ground motion using observed records of just one or two small events. The small events chosen as Green functions to be used in the simulation of the main event are difficult to find. The difference in magnitudes of the small event and the main event must be larger or equal to 1. On the one hand, small events with lower magnitudes could be good candidates to simulate the main event, because by using them as Green functions, the initial rupture point on the fault plane can be indicated accurately. On the other hand, because smaller events are often recorded by very few stations, these events will be damped and lose most of their information on the way reaching the stations.

According to the results, the EGF provides a good alternative for the ground motion simulation in the study region. The simulated strong ground motions show good agreement in comparison with the observed ones. However, some waveforms are underestimated or overestimated and the simulated ground motions can mostly explain major characteristics of the observed records. For instance, in Figure 5, there are differences between the diagrams synthesized using aftershock ($M_{W=}5.6$) and the observed ones. These contrasts between the graphs are seen for the reason that the seismological structures around the epicenters are undefined and site effects in both events were assumed to be the same; besides, the site effects on stations were not eliminated completely. In addition, the EGF method assumes that the two events have the same hypocenter. Therefore, in this technique the focus is on a comparison between the peak values of observed records and the simulated diagrams. In that case, however, there are some dissimilarities between the diagrams, and the values of the maximum acceleration resulting from simulations are rather close to the observed ones. These results show that the strong ground motions can be explained by the average fault rupture model.

The estimated fault plane solution shows strike-slip faulting for the first earthquake and reverse mechanism with a strike-slip component for the second one, which is in agreement with the trend of faults in

the region. Strike, dip and rake of causative faults of the first and second earthquakes were determined as 270, 81 and -175 degrees and 230, 57 and 134 degrees, respectively. These results are in agreement with the focal mechanisms reported by Harvard University.

Considering the fault planes and the distribution of aftershocks, the first rupture initiated from the element (9, 3) on the fault surface at the depth of 9 km and propagated from hypocenter in a unilateral manner from east to west direction. The rupture generated from the second event started at the depth of 7 km, from the element (7, 3) and extended radially from southeast to northwest direction. Moreover, the focal mechanisms of the main shocks showed rupture planes in the same directions as well.

In addition, it should be pointed out that, however, the magnitude of the first earthquake was greater than the magnitude of the second one. The potential hazard the second event could cause was perhaps even more than the first one, not only because the depth of the second earthquake was less than that of the first one but also because structures in the town partially damaged during the first one were likely to be totally destroyed by the second one.

August 11, 2012 earthquakes were the strongest events with magnitude greater than 6 reported over the past 40 years in this region. Therefore, the ground motion characteristics during the mainshocks should be considered for the high safety design of the damaged area.

Reference

Astiz, L., and Kanamori, H., 1984, An earthquake doublet in Ometepec, Guerrero, Mexico: Phys. Earth PlanetInterior, **34**, 24–45.

Cheng, F., and Huang, H., 2011, Strong ground motion simulation of the October 22, 1999 Chiay earthquake using hybrid Green function method: 4th IASPEI international symposium, University of California, Santa Barbara.

Courboulex, F., Virieux, J., Deschamps, A., Gilbert, D., And Zoll, A., 1996, Source investigation of a small event using empirical Green functions and simulated annealing: Geophys. J. Int., **125**, 768–780.

Eshelby, J. D., 1957, The determination of the elastic field of an ellipsoidal inclusion, and related problems: Proc. Roy. Soc., **A241**, 376–396.

Hartzel, S. H., 1978, Earthquake aftershocks as Green functions: Geophys. Res. Lett., **5**, 1–4.

Hutchings, L. and Viegas, G., 2012, Application of Empirical Green Functions in earthquake source, wave propagation and strong ground motion studies: Lawrence Berkeley National Laboratory, USA, 3, 80–130.

Irikura, K., 1991, The physical basis of the empirical Green function method and the prediction of strong ground motion for large earthquake: Proc. International workshop of seismology and earthq. Eng., 89–95.

Kagan, Y. Y., and Jackson, D. D., 1991, Long-term earthquake clustering: Geophys. J. Int., **104**,117–133.

Lay, T., and Kanamori, H., 1980, Earthquake doublets in the Solomon Islands: Phys. Earth Planet. Interior., **21**, 283–304.

Lin, C. H., Yeh, Y. H., Ando, M., Cheng, T. M, and Pu, H. C, 2008, Earthquake doublet sequences: Evidence of static triggering in the strong convergent zones of Taiwan: Terrestrial Atmospheric and Oceanic Sciences, **19**, 589–594.

Miyake, H., Iwata, T, and Irikura, K., 2000, Source characterization of inland crustal earthquakes for near-source ground motions: Proceedings of the 6th international conference on seismic zonation.

Mueller, C., 1985, Source pulse enhancement by deconvolution of an empirical Green function: Geophys. Res. Lett., **12**, 33–36.

Raghu, S. T. G., 2008, Modeling and synthesis of strong ground motion: Department of Civil Engineering, Indian Institute of Technology, Madras, India.

Wells, D. and Coppersmith, K., 1994, New empirical relationships among magnitude, rupture length, rupture width, rupture area and surface displacement: Bulletin of the Seismological Society of America, **8**, 974–1002.